ACS APPLIED MATERIALS & INTERFACES

Research Article

www.acsami.org

Enhanced Thermoelectric Properties of Selenium-Deficient Layered $TiSe_{2-x}$: A Charge-Density-Wave Material

Ranu Bhatt,*[,†] Shovit Bhattacharya,[†] Ranita Basu,[†] Sajid Ahmad,[†,‡] A. K. Chauhan,[†] G. S. Okram,[§] Pramod Bhatt,[∥] Mainak Roy,[⊥] M. Navaneethan,[#] Y. Hayakawa,[#] A. K. Debnath,[†] Ajay Singh,[†] D. K. Aswal,*[,†] and S. K. Gupta[†]

[†]Technical Physics Division, [‡]Astrophysical Sciences Division, [∥]Solid State Physics Division, and [⊥]Chemistry Division, Bhabha Atomic Research Centre, Mumbai 400 085, India

[§]UGC-DAE Consortium for Scientific Research, University Campus, Khandwa Road, Indore 452 001, India

[#]National University Corporation, Research Institute of Electronics, Shizuoka University, 3-5-1 Johoku Naka-ku, Hamamatsu 432 8011, Japan

Supporting Information

ABSTRACT: In the present work, we report on the investigation of low-temperature (300−5 K) thermoelectric properties of hot-pressed $TiSe_2$, a charge-density-wave (CDW) material. We demonstrate that, with increasing hot-pressing temperature, the density of $TiSe_2$ increases and becomes nonstoichiometric owing to the loss of selenium. X-ray diffraction, scanning electron microscopy, and transimission electron microscopy results show that the material consists of a layered microstructure with several defects. Increasing the hot-press temperature in nonstoichiometric $TiSe_2$ leads to a reduction of the resistivity and enhancement of the Seebeck coefficient in concomitent with suppression of CDW. Samples hot-pressed at 850 °C exhibited a minimum thermal conductivity (κ) of 1.5 W/m·K at 300 K that, in turn, resulted in a figure-of-merit (ZT) value of 0.14. This value is higher by 6 orders of magnitude compared to 1.49×10^{-7} obtained for cold-pressed samples annealed at 850 °C. The enhancement of ZT in hot-pressed samples is attributed to (i) a reduced thermal conductivity owing to enhanced phonon scattering and (ii) improved power factor ($\alpha^2\sigma$).

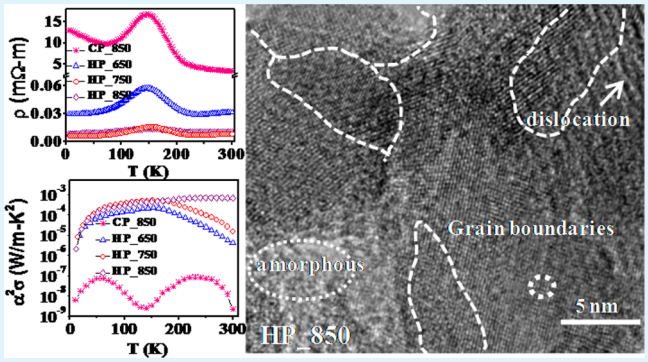

KEYWORDS: *thermoelectric material, layer microstructure, interfaces, lattice thermal conductivity, nanocrystalline materials*

INTRODUCTION

The growing needs of energy sustainability have led to great attention being given to the field of thermoelectric materials because they directly transform waste heat into useful electrical energy. Recent studies on thermoelectric materials have intensively been focused on controlling their microstructural growth in order to obtain optimum electrical and thermal transport properties, i.e., electrical conductivity (σ), Seebeck coefficient (α), and thermal conductivity (κ). An enhanced power factor ($\alpha^2\sigma$) in combination with reduced κ can increase the thermoelectric efficiency of these materials, which is quantified by the dimensionless figure-of-merit ($ZT = \alpha^2\sigma T/\kappa$). The common approaches employed to enhance ZT are: (i) to minimize the thermal conductivity of the material by enhancing the phonon scattering and/or phonon localization while maintaining efficient charge-carrier transport[1−4] and (ii) to enhance the power factor via the quantum confinement of charge carriers using low-dimensional materials.[5,6] Recently, it was proposed that the layered structure of ordered or partially disordered two-dimensional crystalline sheets may exhibit extremely low thermal conductivity.[7,8] Low-dimensional transition-metal dichalcogenides are an interesting class of materials that exist in bulk form as strongly bonded two-dimensional layers, mutually coupled via weak van der Waals forces, forming X−T−X-type structures (where X and T are chalcogen and transition metal, respectively). Several materials of this class also exhibit the formation of charge-density waves (CDWs) at low temperatures.[9−11] During CDW formation, the electron−phonon coupling breaks the translational symmetry of the lattices, creating a perturbed state. This structural perturbation ensues in reducing the thermal conductivity of the materials. The formation of CDW in addition also opens a band gap in the system. Thus, performing band-gap engineering in these systems by either doping/intercalating foreign elements,[12,13] creating off-stoichiometry,[14] or applying external

Received: June 4, 2014
Accepted: October 15, 2014
Published: October 15, 2014

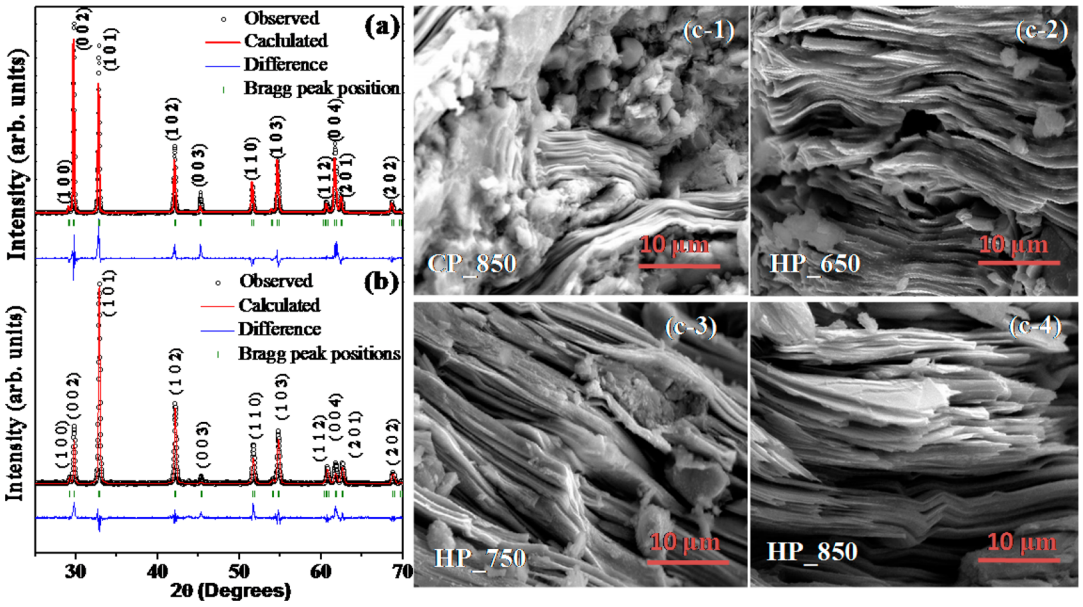

Figure 1. Reitveld-refined XRD patterns of (a) CP_850 and (b) HP_850. SEM images of (c-1) CP_850, (c-2) HP_650, (c-3) HP_750, and (c-4) HP_850.

pressure[15] may be useful in optimizing the thermoelectric properties of these materials.

Titanium diselenide ($TiSe_2$) crystallizes in a 1T layer structure in which titanium is octahedral coordinated by six chalcogen (selenium) atoms. It is not yet clear whether $TiSe_2$ is a semiconductor with a very small indirect gap (0.2 eV)[16,17] or a semimetal with a very small indirect band overlap.[18] This uncertainty may be attributed to the presence of self-doping (due to excess titanium) during the sample preparation. The stoichiometric $TiSe_2$ undergoes a continuous structural phase transition around 202 K, and below this transition temperature, it forms a $2 \times 2 \times 2$ commensurate superlattice, resulting in the formation of a CDW phase.[19] Thus, it is interesting to study $TiSe_2$ to realize the concept of layered disordered crystalline sheets in order to attain improved thermoelectric properties. There are several reports available on the thermoelectric behavior of $TiSe_2$ in which the energy band gap has been altered by introducing transition-metal, alkali-metal, or organic compounds.[13,14] In our previous works, we have demonstrated that intercalation of copper in stoichiometric $TiSe_2$ transforms it from the p-type to the n-type and drastically enhances its thermoelectric properties.[20,21] Apart from doping or intercalation, another possibility to tune the band gap of the material is to alter its stoichiometry by synthesizing the material under different conditions.[22] Such stoichiometric imperfections may strongly influence the thermoelectric properties of $TiSe_2$, which may be useful in device applications.

In the present work, we demonstrate that nonstoichiometry in hot-pressed $TiSe_{2-x}$ drastically improves its thermoelectric performance. It has been found that increasing the hot-press temperature not only suppresses the CDW but also reduces the electrical resistivity. In addition, the room temperature thermal conductivity was found to have been significantly reduced, owing to enhanced phonon scattering due to grain boundaries and defects present in the system. Thus, this study presents the realization of the disordered layer structure concept in $TiSe_{2-x}$ for enhancement of ZT.

EXPERIMENTAL SECTION

Material Synthesis. The polycrystalline $TiSe_2$ samples were prepared using the solid-state reaction method. Stoichiometric amounts of high-purity titanium (5N) and selenium (5N) powders were weighed and vacuum-sealed in a graphite bottle placed inside a silica quartz ampule under a vacuum of $\sim 10^{-5}$ Torr. The materials were subsequently heat-treated at 650 °C for 150 h in a tubular furnace under various heating and cooling steps. Shiny metallic purple-colored powder was obtained, which was further ground using mortar and pestle for a duration of 40 min under an argon ambient atmosphere. The material was then sintered under various conditions: (i) cold-pressed with an applied load of 50 kg, vacuum-sealed (10^{-5} Torr) in a quartz ampule, and sintered at 850 °C for 1 h in a tubular furnace; (ii) hot-pressed at different temperatures, i.e., 650, 750, and 850 °C, under a vacuum of $\sim 10^{-5}$ Torr for 1 h with an applied load of 2.5 kg. These samples are, henceforth, referred to as CP_850, HP_650, HP_750, and HP_850, where CP and HP stand for cold-pressed and hot-pressed samples, respectively. The density of these pellets was measured after different sintering conditions using the Archimedes method.

Characterization. Microstructural and elemental analyses of the prepared samples were carried out using scanning electron microscopy (SEM; Tescan Vega MV2300T/40) and energy-dispersive X-ray analysis (Oxford make, INCA X-act). EDX data were calibrated against standard TiO and a pure selenium element for elemental analysis of $TiSe_2$. High-resolution transmission electron microscopy (HRTEM) images of the samples were captured using a JEOL JEM-2100F microscope. Structural information on the samples was retrieved by Reitveld refinement of the X-ray diffraction (XRD) data recorded using Cu Kα radiation on a Bruker instrument. X-ray photoelectron spectrometry (XPS) spectra were recorded using Mg Kα on DESA-150 electron analyzer (Staib Instruments, Germany) system. The carrier density of the materials was measured using Hall coefficient measurements at 300 K. Four-probe electrical resistivity of the samples was measured in the temperature range of 300−5 K using a Quantum Design CCR. The Seebeck coefficient measurement, in the temperature of 300−5 K, was performed in a commercially available Dewar using the differential direct-current method in a home-built setup. The measurement were carried out by clamping a 10-mm-diameter pellet between the two cylindrical oxygen-free highly conducting copper blocks, which works as a reference material for the thermally generated Seebeck voltage (ΔV). The absolute Seebeck coefficient was calculated by subtracting the copper contribution from the measured sample.

Table 1. Summary of Various Parameters Measured/Calculated for Different $TiSe_{2-x}$ Samples

sample	d (g/cm^3)	x in $TiSe_{2-x}$	c/a	n(300 K) ($\times 10^{20}$ cm^{-3})	ρ(300 K) (mΩ·m)	κ(300 K) (W/m·K)	$\alpha^2\sigma$(300 K) (mW/m·K^2)	ZT(300 K)
CP_850	4.5 ± 0.1	0.11	1.697(2)	0.8	3.4	4.0 ± 0.4	1.99×10^{-6}	1.49×10^{-7}
HP_650	4.7 ± 0.1	0. 2	1.698(2)	1.09	0.032	1.9 ± 0.2	0.004	6.3×10^{-4}
HP_750	5.2 ± 0.1	0.3	1.699(3)	1.14	0.009	3.4 ± 0.3	0.015	0.001
HP_850	5.3 ± 0.1	0.34	1.699(4)	1.69	0.01	1.5 ± 0.1	0.698	0.14

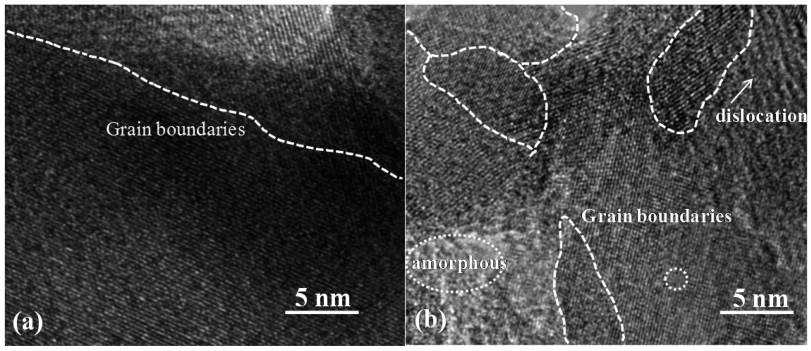

Figure 2. HRTEM images for $TiSe_2$ samples: (a) CP_850; (b) HP_850. Dotted lines represent the grain boundaries. The dislocations and amorphous regions are also marked.

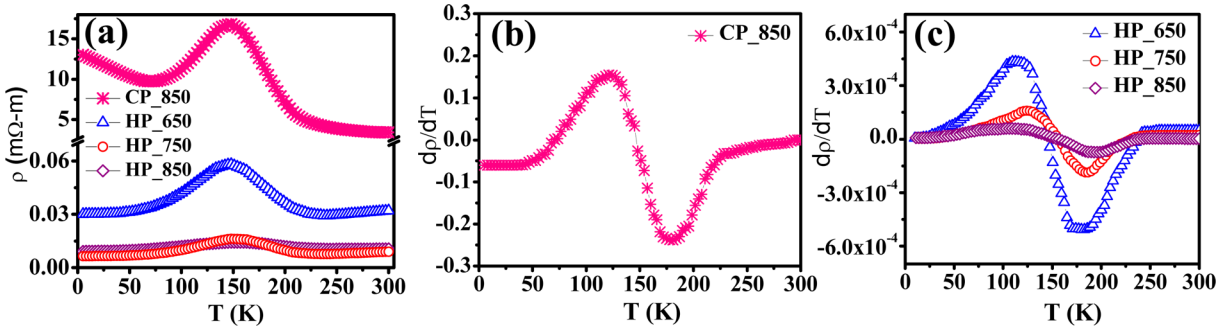

Figure 3. (a) Electrical resistivity plotted against the temperature for samples CP_850, HP_650, HP_750, and HP_850. First-order derivative of the resistivity for (b) CP_850 and (c) HP_650, HP_750, and HP_850.

The data were recorded during the heating cycle. The typical error in the measured α data was less than 4%. The temperature-dependent Raman spectra of the samples were recorded between 300 and 80 K on a Jobin-Yvon Horiba (LabRAM HR800) micro-Raman spectrometer using an argon-ion laser (wavelength = 514.5 nm and power = 400 mW) as an excitation source.

RESULTS AND DISCUSSION

Parts a and b of Figure 1 show the Reitveld-refined XRD patterns for the representative CP_850 and HP_850 samples recorded at room temperature. The XRD patterns refined using space group $P\bar{3}m1$ (No. 164) show that all of the samples exhibit the preferred orientation along the (001) direction; see Figure S1 in the Supporting Information (SI) for details. The change in the refined lattice parameter c/a with increasing hot-pressed temperature is shown in Table 1. It is seen that the c/a ratio of the samples does not have any significant change with the sintering type (i.e., cold or hot pressed) and/or sintering temperature, suggesting no major structural changes in the material. The microstructural growth of the samples is studied by capturing the SEM images of the fractured surface, which are shown in Figure 1c-1−c-4. The SEM image of the CP_850 sample shows the presence of both layered and granular morphology, which are randomly oriented. In the case of hot-pressed samples (i.e., HP_650, HP_750, and HP_850), the morphology becomes predominantly layered in nature with increasing temperature. The layered grains, extending to several microns in length, become denser with increasing temperature. This has the ramification in an enhancement of the sample density, as summarized in Table 1. The density of the CP_850 sample is 4.5 g/cm^3, while the density measured for the HP_850 sample is 5.3 g/cm^3, indicating that hot pressing of the samples reduces the porosity of the materials, as is also seen in the SEM images. The compositions of the samples estimated from the EDX measurements are summarized in Table 1. It is observed that the selenium deficiency (i.e., x in $TiSe_{2-x}$) for the CP_850 samples is 0.11, which increases for hot-pressed samples with increasing hot-press sintering temperature. Analyses of the titanium and selenium XPS spectra (see Figure S2 in the SI) indicate that the binding energies (BEs) of the Ti $2p_{3/2}$ peak of the CP_850 and HP_850 samples are 455.7 and 455.3 eV, respectively. A slight shift in the BE to lower values for the HP_850 samples is attributed to the presence of selenium vacancies. These results also confirm that our samples are not oxidized because the BE of Ti $2p_{3/2}$ in TiO_2 is at a much higher value (~458.5 eV).[23]

Figure 2 shows the HRTEM images for the CP_850 and HP_850 samples. Both of the samples exhibit several randomly oriented polycrystalline grains. However, for the HP_850

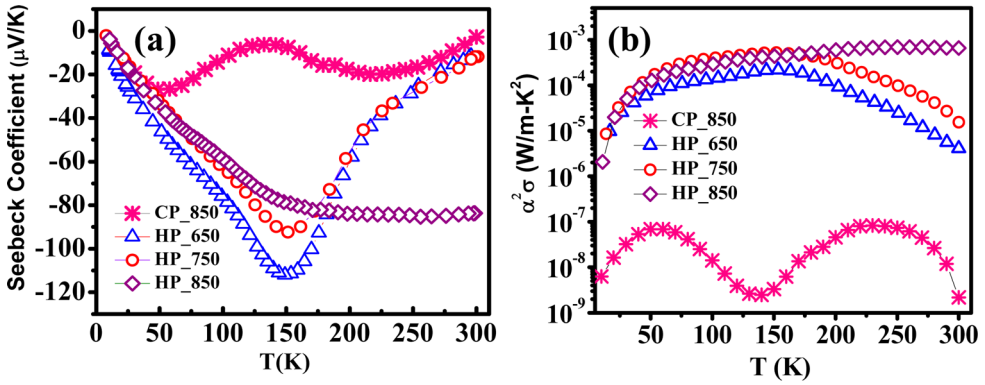

Figure 4. Temperature dependence of (a) the Seebeck coefficient and (b) the power factor ($\alpha^2\sigma$).

sample, additional features, such as twin grain boundaries and a nanoscale amorphous region between the grains, have been observed. These features cover a wide range of the length scale (i.e., from nanoscale to microscale) and may act as scattering centers for the phonons of different mean free paths, which, in turn, may assist in reducing the thermal conductivity of the samples. For example, the defects, dislocations, and nanoscale amorphous regions may provide scattering centers for a small-wavelength phonon (1−10 nm) and the micron-sized grain boundaries of the layered structure may scatter phonons of higher wavelengths.

The temperature dependence of the electrical resistivity ρ(T) shown in Figure 3a, accompanied by a locally peaking electrical resistivity, is regarded as an indicator for the sample quality with respect to the CDW phase transition. This anomaly in resistivity is regarded as a "fingerprint" of the CDW phase characterizing its strength. Di Salvo et al. defined the critical temperature (T_{CDW}) as the local minimum of the first-order derivative dρ/dT and ρ_{max}/ρ(300 K) as an indicator for the sample quality.[19] Stoichiometric $TiSe_2$ is known to possess insulating behavior in the low-temperature regime because of the absence of d-orbital electrons in titanium with T_{CDW} of 202 K. The dρ/dT plots are shown in Figure 3b,c for samples CP_850 and HP_650, HP_750, and HP_850, respectively. It is seen that the minimum in the derivative of the resistivity is found at ∼175 K, which is almost independent of the selenium content in the samples. The obtained T_{CDW} in the present case is in agreement with that reported for nonstoichiometric $TiSe_2$ single crystals.[19] For the CP_850 sample, the resistivity ratio ρ_{max}/ρ(300 K) is found to be 4.7, whereas for the hot-pressed samples with increasing temperature, this ratio gradually decreased to 1.4 (for HP_850), indicating suppression of CDW.

The formation mechanism of CDW in $TiSe_2$ has been under discussion for a long time, and the key aspect about this transition has been the nature of its driving force. In order to explain CDW formation in $TiSe_2$, several mechanisms have been proposed, including the excitonic insulator mechanism,[24,25,27] a band-type Jahn−Teller mechanism,[26] an indirect Jahn−Teller mechanism,[19,27] and the antiferroelectric transition mechanism.[28] In the literature, some experimental support has been found for both the Jahn−Teller mechanism and excitonic insulator mechanism, but there is no conclusive evidence for the dominating mechanism.[27] Recent high-resolution angle-resolved photoemission spectroscopy measurements show evidence of a CDW transition in $TiSe_2$ due to formation of an excitonic condensate.[29] At temperatures greater than T_{CDW}, the electronic structure of $TiSe_2$ near the Fermi energy (E_F) consists of a valence band (Se 4p) close to the Γ and L points and a conduction band (Ti 3d) at the L point, which slightly overlap through an indirect gap. However, at temperatures below T_{CDW}, formation of a 2 × 2 × 2 superlattice takes place, and L points are back-folded into the zone center. The formed excitons (bound electron−hole pair) condense into a new macroscopic state and induce a new periodicity in the system. The excitons can be broken easily by thermal energies, and hence they only exist at low temperatures. In the present case, CDW formation is predominant in the CP_850 samples owing to their compositions close to that of stoichiometric $TiSe_2$. However, in hot-pressed samples, particularly in HP_850 samples, the CDW vanishes, owing to the selenium loss. The loss of selenium indicates that the sample is self-doped with excess titanium, and indeed the Hall coefficient measurements show that these samples are n-type semiconductors. The titanium cationic vacancies shift the E_F level deeper into the conduction band (Ti 3d), resulting in increased electron charge carriers. Table 1 summarizes the electron concentration (n) as a function of x in $TiSe_{2-x}$. The sample HP_850 exhibits the highest charge-carrier density of 1.69 × 10^{20}/cm^3. In the HP_850 sample, enhanced charge-carrier density not only leads to suppression of CDW but also reduces the room temperature electrical resistivity, as summarized in Table 1. It is also a fact that improved grain growth and densification of the material under hot-pressing conditions contribute to the lowering of the electrical resistivity.

Figure 4a shows the temperature-dependent Seebeck coefficient (α) behavior for different samples. For all of the samples, α is negative in the entire temperature range, confirming that samples exhibit an n-type semiconducting nature and electrons are the majority charge carriers. Also, the room temperature α value increases with x in $TiSe_{2-x}$. For the CP_850 sample, the room temperature α value is only −2.6 μV/K and exhibits complex nonmonotonic temperature dependence. Because the material in this case is close to stoichiometric $TiSe_2$, both holes in the Se 4p band and electrons in Ti 3d contribute to the thermoelectric power. A small dip in α at 150 K is attributed to the existence of CDW formation, while the peak at ∼55 K corresponds to the phonon drag of charge carriers caused by moving of the charge carriers under phonon flow action due to electron−phonon coupling. For the HP_650 and HP_750 samples, α exhibits a maximum value at 150 K, which coincides with the CDW transition observed in the resistivity, indicating that the CDW phase is responsible for nonmonotonic temperature dependence.

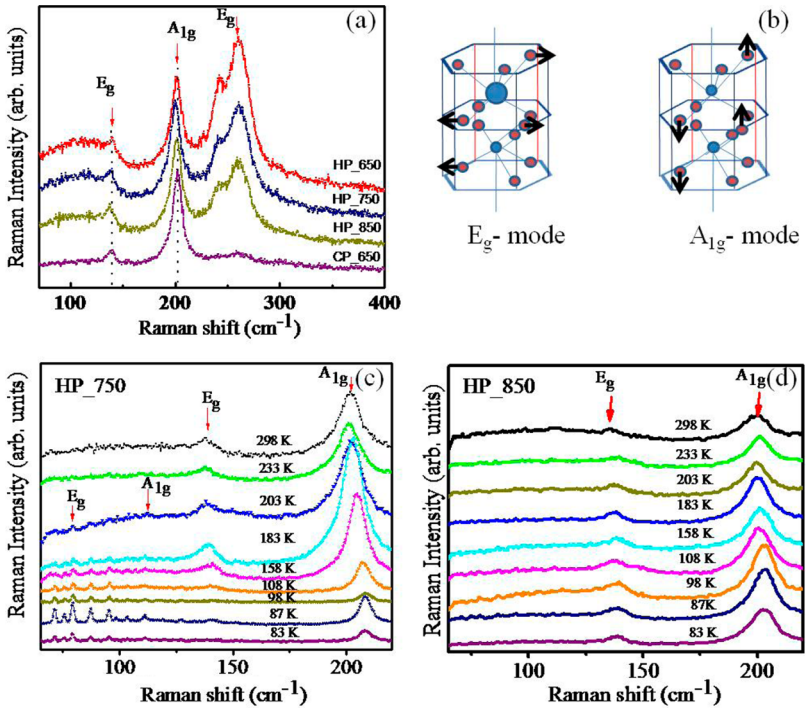

Figure 5. (a) Raman spectra of sintered $TiSe_{2-x}$ samples recorded at 300 K. (b) Raman-active E_g and A_{1g} modes in the crystal structure of 1T-$TiSe_{2-x}$. (c) Temperature-dependent Raman spectra of the HP_750 sample exhibiting CDW features. (d) Temperature-dependent Raman spectra of the HP_850 sample showing the absence of CDW features.

However, for the HP_850 sample, α is exceptionally large (−83.8 μV/K) at room temperature and decreases monotonically with decreasing temperature, which indicates that CDW is suppressed because of enhanced electron density caused by titanium doping. Figure 4b shows the temperature dependence of the power factor calculated for all of the samples. Samples sintered in a vacuum hot press shows 4−6 orders of improvement in the power factor value compared to that of the CP_850 sample.

CDW formation in $TiSe_2$ is associated with structural disorder, transforming the system to the commensurate state, where the translational symmetry of the lattice is destroyed and forms a new superlattice of 2 × 2 × 2. This has a drastic effect on the number of vibrational spectra of the crystal and the number of Raman-active modes. Because Raman is inelastic, scattering of light by phonons thus requires wave-vector conservation, allowing only zone center excitation to participate in the first-order Raman scattering. The imposition of a commensurate superlattice on the lattice reduces the size of the Brillouin zone, folding the dispersion curves of the various propagating excitations back into the center of zone. $TiSe_2$ exhibits space group $P\bar{3}m1$ with spectroscopic symmetry D_3d^3, implying that there is one formula, i.e., N = 3 atoms per elementary unit cell. According to Jaswal, disintegration of the displacement of three atoms into irreducible representations yields nine zero-center (Γ-point) vibrational modes for $TiSe_2$.[30]

$$\Gamma = A_{1g} + E_g(2) + 2A_{2u} + 2E_u(2) \quad (1)$$

This includes two Raman-active Γ-point phonon modes of A_{1g} in which two selenium atoms per unit cell move relative to one another along the z axis and a doubly generate E_g mode in which selenium atoms move to one another along the x or y axis, as shown in Figure 5b. Figure 5a shows the Raman spectra of the samples measured at 300 K. The peaks at 134 and 202 cm^{-1} correspond to the E_g and A_{1g} modes, respectively. The broad peak at 260 cm^{-1} may be assigned to the two-phonon process. Sintering the sample under hot-press conditions evolves this peak significantly and allows it to exist even up to a hot-press temperature of 850 °C. The transition to the CDW regime results in formation of a superlattice with space group D_4d^3, which contains N = 24 atoms, i.e., eight formula units per unit cell. The three translational vectors thus would generate $3N$ = 72 zone center normal modes having irreducible representations as follows:[31]

$$\Gamma = 5A_{1g} + 7A_{2g} + 12_{Eg} + 5A_{1u} + 7A_{2u} + 12E_u \quad (2)$$

Temperature-dependent Raman spectra are shown in Figure 5c,d for the HP_750 (CDW exists) and HP_850 (CDW vanishes) samples. It is observed that, in the case of the 750 °C sintered sample, several new modes start to appear below 134 cm^{-1} from the beginning of the CDW transition temperature. The original E_g and A_{1g} modes at 134 and 202 cm^{-1} still exist; however, a slight blue shift in their position and suppression in their intensity have been observed at low temperature. The new existing Raman mode, designated as the CDW phonon mode, is enhanced as the temperature reaches the value of CDW formation. The CDW phonon mode exists up to the lowest measurement temperature of 80 K. However, in the case of the sample HP_850, no signature of CDW phonon modes is observed, and all of the original Raman modes exist up to 80 K.

The ZT value of all the samples synthesized at 300 K have been estimated by measuring their κ values. Table 1 summarizes the κ and ZT values calculated for all $TiSe_{2-x}$ samples. The CP_850 sample exhibits a comparatively high κ value of 4 W/m·K; however, sintering the sample under hot-press conditions significantly reduces the κ value. A minimum κ of 1.5 W/m·K was achieved for the HP_850 sample. The thermal conductivity of the sample mainly depends on the

mobility of the electron and phonon in the sample. When κ is quantified per Weidmann–Franz law ($\kappa_{ph} = \kappa - \kappa_e$), the minimum phonon contribution to κ is achieved for the HP_850 sample, which is attributed to the scattering of phonons of all wavelengths by micron-sized and nanosized grain boundaries, amorphous regions, and atomic defects because of the selenium loss. The ZT calculated for the CP_850 sample is 1.49×10^{-7} at 300 K. Interestingly, because of reduced κ and improved $\alpha^2\sigma$, a maximum ZT value of 0.14 is achieved for the HP_850 sample, which is higher by 6 orders of magnitude compared to that of the CP_850 sample.

CONCLUSIONS

The thermoelectric properties of $TiSe_2$ are very sensitive to the stoichiometry of the sample. The formation of CDW in $TiSe_{2-x}$ has been asserted based on the local peak in the temperature-dependent electrical resistivity at ~175 K, as well as temperature-dependent Raman spectroscopy. An increase in the hot-pressed temperature during synthesis of $TiSe_{2-x}$ induces cationic vacancies due to loss of selenium. The increased electron density due to self-doping of titanium not only suppresses the CDW but also reduces the electrical resistivity. In addition, the Seebeck coefficient was found to increase. The HP_850 sample exhibits a κ value of 1.5 W/m·K (at 300 K), leading to a ZT value of 0.14, which is higher by 6 orders of magnitude compared to 1.49×10^{-7}, obtained for the CP_850 sample. The enhanced ZT value of the HP_850 sample is attributed to a reduced thermal conductivity and an improved power factor ($\alpha^2\sigma$). This study presents the realization of the disordered layer structure concept in $TiSe_{2-x}$ for enhancement of ZT, which can be implemented for other such systems.

ASSOCIATED CONTENT

Supporting Information

Fitted XPS spectra of the CP_850, HP_650, HP_750, and HP_850 samples, Reitveld-refined XRD patterns, and structural parameters of the $TiSe_{2-x}$ samples. This material is available free of charge via the Internet at http://pubs.acs.org.

AUTHOR INFORMATION

Corresponding Authors

*E-mail: rbhatt@barc.gov.in.
*E-mail: dkaswal@barc.gov.in.

Notes

The authors declare no competing financial interest.

REFERENCES

(1) Sales, B. C. Electron Crystal and Phonon Glasses: A New Path to Improved Thermoelectric Materials. *Mater. Res. Soc. Bull.* **1998**, *23*, 15–21.
(2) Venkatasubramanian, R.; Siivola, E.; Colpitts, T.; O'Quinn, B. Thin-film Thermoelectric Devices with High Room-temperature Figure of Merit. *Nature* **2001**, *413*, 597–602.
(3) Synder, G. J.; Christensen, M.; Nishibori, E. J.; Calliat, T.; Iversen, B. B. Disordered Zinc in Zn_4Sb_3 with Phonon-glass and Electron Crystal Thermoelectric Properties. *Nat. Mater.* **2004**, *3*, 458–463.
(4) Wölfing, B.; Kloc, C. T. J.; Bucher, E. High Performance Thermoelectric Tl_9BiTe_6 with an Extremely Low Thermal Conductivity. *Phys. Rev. Lett.* **2001**, *86*, 4350–4353.
(5) Dresselhaus, M. S.; Chen, G.; Tang, M. Y.; Yang, R. G.; Lee, H.; Wang, D. Z.; Ren, Z. F.; Fleurial, J.-P.; Gogna, P. New Directions for Low-dimensional Thermoelectric Materials. *Adv. Mater.* **2007**, *19*, 1043–1053.
(6) Lin, M.-Y.; Dresselhaus, M. S. Thermoelectric Properties of Superlattice Nanowires. *Phys. Rev. B* **2003**, *68*, 075304.
(7) Chiritescu, C.; Cahill, D. G.; Nguyen, N.; Jhonson, D.; Bodapati, A.; Keblinski, P.; Zschack, P. Ultralow Thermal Conductivity in Disordered Layered WSe_2 Crystals. *Science* **2007**, *315*, 351–353.
(8) Bhattacharya, S.; Basu, R.; Bhatt, R.; Pitale, S.; Singh, A.; Aswal, D. K.; Gupta, S. K.; Navaneethan, M.; Hayakawa, Y. $CuCrSe_2$: A High Performance Phonon Glass and Electron Crystal Thermoelectric Material. *J. Mater. Chem. A* **2013**, *1*, 11289–11294.
(9) Sipos, B.; Kusmartseva, A. F.; Akrap, A.; Berger, H.; Forró, L.; Tutiš, E. From Mott State to Superconductivity in 1T-TaS_2. *Nat. Mater.* **2008**, *7*, 960–965.
(10) Gordon, R. A.; Yang, D.; Crozier, E. D.; Jiang, D. T.; Frindt, R. F. Structure of Exfoliated Single Layers of WS_2, MoS_2 and $MoSe_2$ in a Aqueous Suspension. *Phys. Rev. B* **2002**, *65*, 125407.
(11) Kuc, A.; Zibouche, N.; Heine, T. Influence of Quantum Confinement on the Electronic Structure of the Transition Metal Sulphide TiS_2. *Phys. Rev. B* **2011**, *83*, 245213.
(12) Morosan, E.; Zandbergen, H. W.; Dennis, B. S.; Bos, J. W. G.; Onose, Y.; Klimczuk, T.; Ramirez, A. P.; Ong, N. P.; Cava, R. J. Superconductivity in Cu_xTiSe_2. *Nat. Phys.* **2006**, *2*, 544–550.
(13) Kuranov, A. V.; Pleshchev, V. G.; Titov, A. N.; Baranov, N. V.; Krasavin, L. S. The Effect of Intercalation by 3d Elements on the Structure and Physical Properties of Titanium Diselenide M_xTiSe_2 (M = Cr, Fe, Co). *Phys. Solid State* **2000**, *42*, 2089–2092.
(14) Levy, F. The Influence of Impurities on the Electrical Properties of $TiSe_2$ Single Crystals. *J. Phys. C: Solid State Phys.* **1980**, *13*, 2901.
(15) Kusmartseva, A. F.; Sipos, B.; Berger, H.; Forrò, L.; Tutiš, E. Pressure Induced Superconductivity in Pristine 1-T $TiSe_2$. *Phys. Rev. Lett.* **2009**, *103*, 236401.
(16) Anderson, O.; Karschnick, G.; Manzke, R.; Skibowski, M. The Phase Transition in the Electronic Strucutre of 1T-$TiSe_2$. *Solid State Commun.* **1985**, *53*, 339.
(17) Rasch, J. C. E.; Stemmler, T.; Müller, B.; Dudy, L.; Manzke, R. 1T-$TiSe_2$ Semimetal or Semiconductor? *Phys. Rev. Lett.* **2008**, *101*, 237602.
(18) Kidd, T. E.; Miller, T.; Chou, M. Y.; Chiang, T.-C. Electron-hole Coupling and the Charge Density Wave Transition in $TiSe_2$. *Phys. Rev. Lett.* **2002**, *88*, 226402.
(19) Di Salvo, F. J.; Moncton, D. E.; Waszczak, J. V. Electronic Properties and Superlattice Formation in Semimetal $TiSe_2$. *Phys. Rev. B* **1976**, *14*, 4321.
(20) Bhatt, R.; Basu, R.; Bhattacharya, S.; Singh, A.; Aswal, D. K.; Gupta, S. K.; Okram, G. S.; Ganesan, V.; Venkateshwarlu, D.; Sürger, C.; Navneethan, M.; Hayakawa, Y. Low Temperature Thermoelectric Properties of Cu Intercalated $TiSe_2$: A Charge Density Wave Material. *Appl. Phys. A: Mater. Sci. Process.* **2013**, *111*, 465–470.
(21) Bhatt, R.; Bhattacharya, S.; Patel, M.; Basu, R.; Singh, A.; Sürger, C.; Navaneethan, M.; Hayakawa, Y.; Aswal, D. K.; Gupta, S. K. Thermoelectric Performance of Cu Intercalated Layered $TiSe_2$ above 300 K. *J. Appl. Phys.* **2013**, *114*, 114509.
(22) Hilderbrand, B.; Didiot, C.; Novello, A. M.; Monney, G.; Scarfato, A.; Ubaldini, A.; Berger, H.; Bowler, D. R.; Renner, C.; Aebi, P. Doping Nature of Native Defects in 1T-$TiSe_2$. *Phys. Rev. Lett.* **2014**, *112*, 197001.
(23) http://srdata.nist.gov/xps/.
(24) Wilson, J. A.; Mahajan, S. The Anamalous Behaviour of $TiSe_2$ and the Excitonic Insulator Mechanism. *Commun. Phys.* **1977**, *23*, 2.
(25) van Wezel, J.; Nahai-Williamson, P.; Saxena, S. S. Exciton–phonon-driven Charge Density Wave in $TiSe_2$. *Phys. Rev. B* **2010**, *81*, 165109.
(26) Cercellier, H.; Monney, C.; Clerc, F.; Battaglia, C.; Despont, L.; Garnier, M. G.; Beck, H.; Aebi, P.; Patthey, L.; Berger, H.; Forro, L. Evidence for an Excitonic Insulator Phase in 1T-$TiSe_2$. *Phys. Rev. Lett.* **2007**, *99*, 146403.

(27) Hughes, H. P. Structural Distortion in $TiSe_2$ and Related Materials—A Possible Jahn–Teller Effect. *J. Phys. C: Solid State Phys.* **1977**, *10*, L319.
(28) White, R. M.; Lucovsky, G. Suppression of Antiferroelectricity in $TiSe_2$ by Excess Carriers Nuovo Cimento. *Soc. Ital. Fis. B* **1977**, *B38*, 280.
(29) Monney, C.; Cercellier, H.; Clerc, F.; Schwier, E. F.; Didiot, C.; Garnier, M. G.; Beck, H.; Aebi, P.; Berger, H.; Forro, L.; Patthey, L. Spontaneous Exciton Condensation in 1T-$TiSe_2$: BCS-like Approach. *Phys. Rev. B* **2009**, *79*, 045116.
(30) Jaswal, S. S. Lattice Dynamics of $TiSe_2$. *Phys. Rev. B* **1979**, *20*, 5297.
(31) Holy, J. A.; Woo, K. C.; Klein, M. V.; Brown, F. C. Raman and Infrared Studies of Superlattice Formation in $TiSe_2$. *Phys. Rev. B* **1977**, *16*, 3628.